Neck growth kinetics during polymer sintering for powder-based processes

Juan E. Alvarez[1*], *Henk* Snijder[2], *Tom* Vaneker[2], *Hongyang* Cheng[1], *Stefan* Luding[1**], and *Thomas* Weinhart[1***]

[1]Multi-Scale mechanics group, Engineering Technology, MESA+, University of Twente. The Netherlands.
[2]Manufacturing Systems group, Engineering Technology, MESA+, University of Twente. The Netherlands.

Abstract. To prevent texture defects in powder-based processes, the sintering time needs to be adjusted such that a certain amount of coalescence is achieved. However, predicting the required sintering time is extremely challenging to assess in materials such as polymers because the kinetics exhibit both elastic and viscous characteristics when undergoing deformation. The present work introduces a computational approach to model the viscoelastic effect in the sintering of particles. The model contains three stages, three different mechanisms driven by adhesive inter-surface forces and surface tension, which describes the non-linear sintering behaviour. Experimental data from the binary coalescence of Polystyrene (PS), Polyamide (PA) 12 and PEEK 450PF particles are employed to calibrate the contact model, as implemented in MercuryDPM, an open-source software package. Using machine learning-based Bayesian calibration, good agreement is obtained between the experimental data and the numerical results. The findings will be used in future studies to predict densification rates in powder-based processes.

1 Introduction

Recently, industries have shown interest in powder-based processes because complex objects can be created. These processes start with the deposition of a large number of particles on a building platform. A laser is set to heat the particle surfaces to sinter them at the contact points. Thereby, a solidified surface layer is created, which is augmented with new depositions of particles and their respective sintering. To control the sintering among the particles, the sintering time is set according to the laser specifications. However, if the setup barely satisfies the material conditions, non-sufficient or excessive time is required to complete the neck growth. Therefore, the created object may display texture defects such as delamination, distortion, and dimensional inaccuracies.

In order to prevent texture defects in powder-based processes, the neck growth kinetics needs to be model accurately. Although the literature provides different contact models for the prediction of sintering neck growth [1, 2], the complexity of the viscoelastic response in materials such as polymers hinders the correct estimation [3]. First, polymers properties change according to the molecular weight and temperature. Second, the contact area differs from the stress-free volume element in the bulk. It leads that the viscoelastic behaviour at the interface exhibits retardation for stress-relaxation, which lags the sintering for a considerable time interval. Initially, Frenkel [1] proposed that the sintering rate was driven by surface tension and accommodated by viscous flow. However, simulations based on Frenkel's model disagree with reported experiments on the sintering of polymer particles [4-6]. The reason is that a simple power-law modestly describes the complex viscoelastic behaviour in polymer sintering. It was demonstrated by Fuchs *et al*. [4] that additional driving mechanisms should be included in the discrete contact model in order to predict the sintering time accurately. To overcome this fact, Lin *et al*. [7] introduced to the prediction of sintering time a time-dependent neck growth approach, which relies on three sintering mechanisms. First, the JKR model based on the global energy balance is utilized, which equates the work of adhesion to the change of potential energy [8]. Second, the neck-growth is driven by adhesive inter-surface forces and it is accommodated by visco-elastic deformation. Third, the sintering mechanism proposed by Frenkel takes place to drive the coalescence forward. Thus, an accurate neck growth kinetics in polymers can be described.

This work presents a computational approach to include the model proposed by Lin *et al*. [7] in MercuryDPM [10], and it contrasts the simulation results with experimental data of PS particles, which was initially studied by Hejmadly *et al*. [11], PA12 particles sintered in our own experiments, and PEEK 450PF particles presented by Beretta *et al*. [5]. Due to the micro-mechanical calibration remains a tremendous challenge because the diversity of granular materials, this work utilizes a Bayesian calibration technique proposed by Cheng *et al*. [12].

*e-mail: j.e.alvareznaranjo@utwente.nl
**e-mail: s.luding@utwente.nl
***e-mail: t.weinhart@utwente.nl

A video is available at https://doi.org/10.48448/yd0b-3e66

2 Numerical modelling

To model the sintering of bulk materials, the discrete particle method (DPM) is highly suitable. DPM simulates the motion of discrete particles using Newton's laws. Particles are assumed to be rigid and interact via a contact model. In this work, we apply the elasto-plastic and dissipative model proposed by Luding [9], which is implemented in MercuryDPM [10]. Fig. 1 illustrates the contact model.

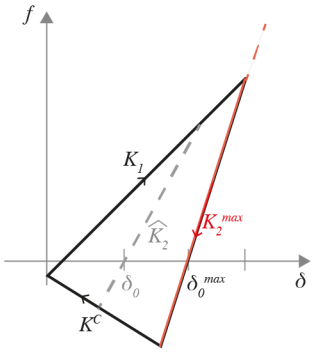

Figure 1. Visco-elasto-plastic contact Law. If $\delta_0 > \delta_0^{max}$ the overlap enters to the "complete melting" of the particles.

The elasto-plastic and dissipative model computes the repulsive elasto-plastic forces during compression (loading) between the particles using a loading stiffness K_1. The unloading process follows the slope of $\hat{K}_2$, which varies between K_1 and K_2^{max}, depending on δ_0, which reproduces the plastic effect. If the equilibrium overlap δ_0 becomes larger than δ_0^{max}, the stiffness becomes equal to K_2^{max} and the force remains on the corresponding fluidity branch with the same slope[1]. After the contact force becomes negative, for $\delta < \delta_0$, the model introduces cohesive forces using the cohesion stiffness K^c. Thus, the normal force f^n between two particles in contact ($\delta > 0$) describes the interaction as

$$f^n = -f_a + \left\{ \begin{array}{ll} K_1\delta & \text{if } \delta = \delta_{max} \\ \hat{K}_2(\delta - \delta_0) & \text{if } \delta_{min} \le \delta < \delta_{max} \\ K^c\delta & \text{if } \delta < \delta_{min} \end{array} \right\} - \gamma^n v^n, \tag{1}$$

The overlap δ defines the deformation measurement as

$$\delta = (R_i + R_j) - (\mathbf{r}_i - \mathbf{r}_j) \cdot \mathbf{n}, \tag{2}$$

where R_i and R_j are particle radii. $\mathbf{r}_i$ and $\mathbf{r}_j$ are the particle positions with unit vector $\mathbf{n} = (\mathbf{r}_i - \mathbf{r}_j)/|\mathbf{r}_i - \mathbf{r}_j|$. The adhesive force f_a is assumed constant, and γ^n represents a viscous dissipation coefficient. Fuchs *et al.* [4] extended this model to simulate sintering by introducing the rate of plastic overlap, $\dot{\delta}_0$. This rate was chosen to satisfy Frenkel's approximation, i.e. $\delta_0/R = t/\tau_s$, where τ_s denotes the sintering time.

[1]It reduces unrealistic large overlaps, approximating the melt incompressibility with a rather low stiffness, in order to have the computation time-step not too small.

Here, we modify the calculation of $\dot{\delta}_0$ such that it agrees with the framework proposed by Lin *et al.* [7]. The authors modelled the evolving contact radius by defining it as the maximum of three different models, $a = \max(a_0, a_1, a_2)$, each of which describes a different stage of the coalescence process. An illustrative sintering regime map is presented in Fig. 2.

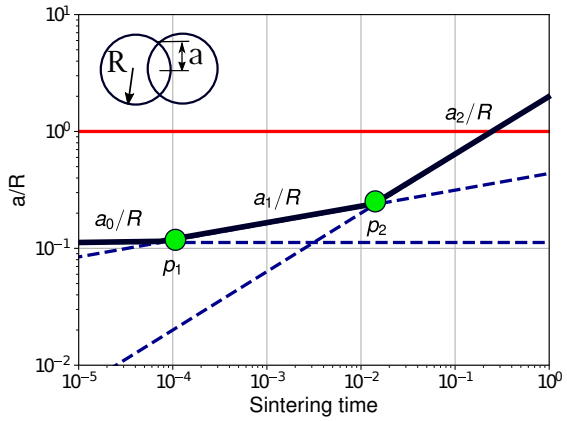

Figure 2. Regime map for three different sintering mechanisms. First, an adhesive equilibrium is modelled before point p_1, following the JKR flat zone. From point p_1 to point p_2, it is defined the starting point at which the instantaneous compliance of the material takes place, and after point p_2, the material is sufficiently relaxed to flow under surface tension.

In the first stage, it is assumed that the adhesion between the particle surfaces causes a flattened contact independent on time [8]. This results in a constant contact radius a_0, defined as

$$\frac{a_0}{R} = \left(\frac{9\pi C_0 W}{2R}\right)^{1/3}, \tag{3}$$

where W is the work of adhesion. Since the particles are identical, $W = 2\gamma$. $C_0 = 1/2E$, is the elastic instantaneous compliance, often denoted as J_0.

The second sintering mechanism displayed in Fig. 2 is denominated "zipping" and the contact radius a_1 grows driven by adhesive inter-surface forces and it is accommodated by viscoelastic deformation [7]. The rate of neck growth a/R is estimated as

$$\frac{a_1}{R} = \left(\frac{63\pi^3}{16}\right)^{1/7}\left(\frac{\delta_c}{R}\right)^{2/7}\left(\frac{2C_1\gamma t}{R}\right)^{1/7}, \tag{4}$$

where C_1 is related to a material property, and it is called in our work as fluidity. δ_c represents the cut-off distance at which the adhesive traction vanishes. The third and final mechanism is denominated "stretching" and the contact radius a_2 grows driven by surface tension and it is accommodated by viscous flow (Frenkel's approximation). It is defined as

$$\frac{a_2}{R} = \left(\frac{t}{\tau_s}\right)^{1/2}, \tag{5}$$

where $\tau_s = \eta R/\gamma = R/8C_1\gamma$, is the characteristic sintering rate, and η defines the viscosity. Recognizing that friction forces act in the tangential direction, they do not sig-

nificantly affect the normal forces calculated via this approach. The differential equations of particle Newtonian movements are solved numerically using the Velocity-Verlet algorithm.

3 Experimental acquisitions and DPM calibration

Three experiments on sintering were employed to analyse the neck growth behaviour. First, experimental data on PS particles were taken from Hejmady *et al.* [11]. Second, PA12 particles were sintered using a hot-stage microscope (see Fig. 3). Finally, reported experimental observations on 450PF particles were utilized [5].

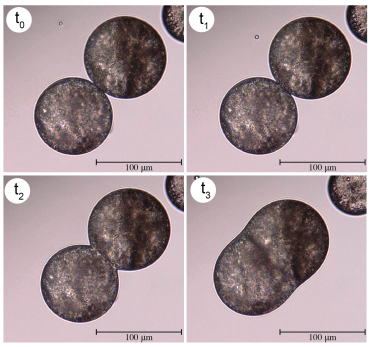

Figure 3. Snaphots from binary coalescence experiments with PA12 particles at different times, $t_0 = 0.0$ (a/R): contact point, $t_1 : 0.1$ (a/R), $t_2 = 0.2$ (a/R), $t_3 = 0.8$ (a/R).

Table 1 lists the material properties of the polymers.

Table 1. Material properties

Property	PS	PA12	PEEK 450PF
R [μm]	30.5	31.5	25.0
E [GPa]	1.60	1.65	2.00
γ [mN/m]	35.0	40.70	41.0

In order to model the neck-growth kinetics, the DPM simulations contain a pair of 3D particles of equal diameter. Frictional and gravitational forces are neglected approaching the simulation to the experimental environment. It contains an oil layer to minimize the inertia between the particles and the glass plate. The particles are set just in contact at t_0. Furthermore, an initial adhesive force, $f_a = K_1 * 1.0 \times 10^{-3}$ m, is set to quickly reach the initial equilibrium radius a_0. the rate of plastic overlap $\dot{\delta}_0$ is set to reach the contact radius $a = \sqrt{\delta R}$ in accordance to eq. (3), (4), (5). All simulations are set using the properties listed in Table 2.

Table 2. System properties

ρ [Kg/m^3]	K_1 [N/m]	K_2^{max} [N/m]	K_c [N/m]
1000	3.0×10^{-4}	10.0 K_1	1.0 K_1

δ_0^{max} is set such that final, fully merged particles have a contact radius $a_f = \sqrt[3]{2}$, which corresponds to the final radius of two intersecting spheres. For this, $\delta_0^{max} = \phi 2R_{ij}$, where $\phi = a_f$. This leaves three material parameters, which are not yet characterised: sintering time τ_s, fluidity C_1, and adhesive cut-off distance δ_c. We will use the experimental data to calibrate these parameters, utilizing the Bayesian calibration software "GrainLearning" to explore the interdependence among the parameters [12]. GrainLearning uses the recursive Bayes' rule to update the probability of model parameters with observational data. The process is repeated with an iterative refined proposal density to solve the inverse problem[2]. Table 3 presents the best likelihood estimation of the three aforementioned parameters.

Table 3. Properties for DPM calibration

Property	PS	PA12	PEEK 450PF
C_1 [Pa^{-1}s^{-1}]	21.2	4.1×10^{-1}	1.5×10^{-1}
τ_s [s]	2.1×10^{-6}	1.2×10^{-4}	5.7×10^{-4}
δ_c [m]	4.8×10^{-7}	2.7×10^{-7}	9.8×10^{-7}

4 Results and discussion

The first neck-growth estimation corresponds to the sintering of PS particles. The simulation result is depicted in Fig. 4.

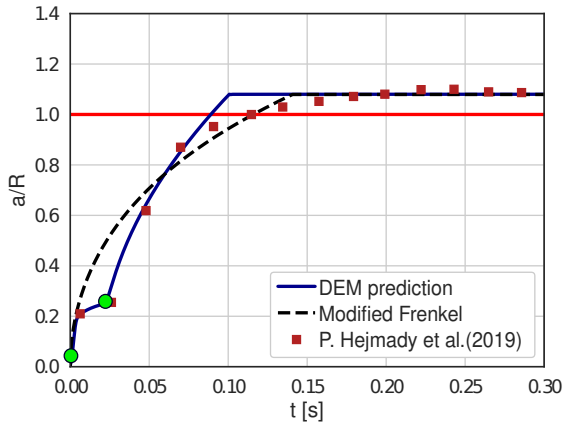

Figure 4. sintering curve of Polystyrene particles, $R = 30.0$ μm compared with Frenkel's model (dashed line), and experimental data (boxes) [4].

The simulation result in Fig. 4 is plotted against the experimental data reported by Hejmady *et al.* [11]. An important consequence for sintering in polymer materials comes from the fact that particles with less molecular weight and small particles radius are expected to sinter faster [3]. This is the case for PS, in which the stress relaxation comes immediately at 0.03 s. Thereafter, the viscous flow mechanism for sintering dominates the process. It is demonstrated with the comparison against the modified Frenkel's model that it overpredicts the experimental data, and it agrees after 0.11 s of the coalescence. Fuchs *et*

[2]The inverse problem in our case is the estimation of particle-scale parameters from particle dynamics, such as neck-growth kinetics

al. [4] supported that the sintering is assisted by different mechanisms before the relaxation time takes place.

The second neck-growth prediction corresponds to the sintering of PA12 particles. The simulation result is presented in Fig. 5.

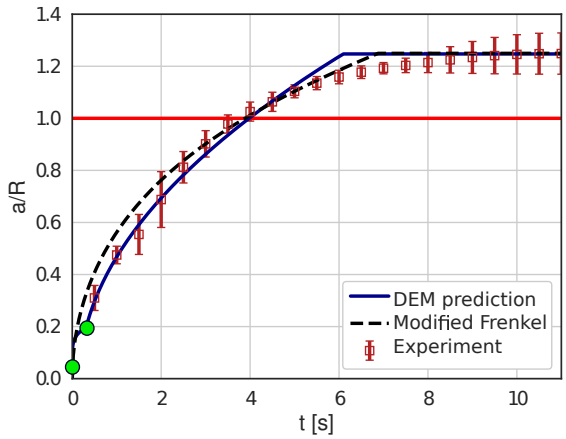

Figure 5. Sintering curve of PA12 particles, $R = 31.5\ \mu$m compared with Frenkel's model (dashed line), and experimental data (boxes).

The results show the the non-linear coalescence path. The transition between the second and third sintering mechanism is at 0.4 s, when $a/R \approx 0.2$. The maximum overlap ($a/R = 1.0$) is achieved at $t = 4.0$ s. After this point, particles merge until complete the coalescence, $a = \sqrt[3]{2R}$, is reached at 6.1 s. It indicates that the coalescence of PA12 particles exhibits different sintering rates, which cannot be neglected to reproduce the experimental observations. Frenkel's model only approaches the experimental data after the 100% of coalescence.

The third case of study corresponds to the binary coalescence of PEEK 450PF particles. The result of the neck-growth is depicted in Fig. 6.

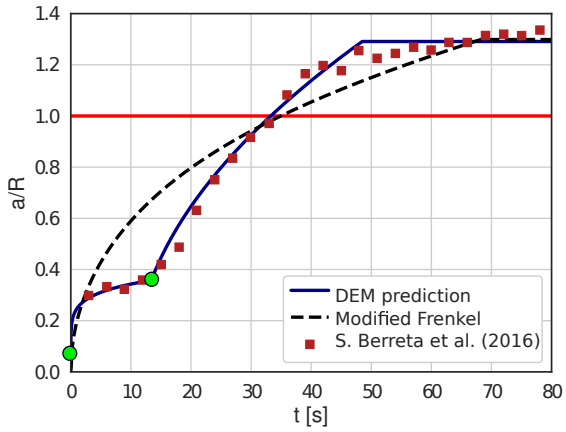

Figure 6. sintering curve of PEEK 450PF particles, $R = 25.0\ \mu$m compared with Frenkel's model (dashed line), and experimental data (boxes) [5].

Fig. 6 illustrates the implication of polymers with high viscosity for sintering. The delay to reach the stress relaxation is about 14.0 s and it takes into account 40% of the coalescence. Frenkel's model overpredicts the experimental results, leading to an inaccurate measurement of the sintering time.

5 Conclusions

In order to prevent surface defects in powder-based processes, the sintering time needs to be controlled. As a consequence, the neck growth kinetics requires to be estimated with a good agreement. This study provided an approach to evaluate the neck growth kinetics based on three different mechanisms, specifically for polymer powders. Our approach only requires the calibration of three micro parameters: (1) sintering time, (2) adhesive cut-off distance, and (3) fluidity. It leads to a simplification in the discrete particle predictions. The sintering model, implemented in the open-source code MercuryDPM, is calibrated against experimental data via GrainLearning software. An increase in the modelling accuracy is obtained compared with traditional ones. The findings provide an important insight into the nature of sintering, and a reliable contact model to predict sintering time. The results will be utilized in future studies to model and validate densification rates of powder-based processes.

This work was financially supported by NWO-TTW project No.16604 Virtual Prototyping of Particulate Processes (ViPr) – Design and Optimisation via Multiscale Modelling and Rapid Prototyping.

References

[1] J. Frenkel, J. Phys. **9**, 385 (1945)
[2] K. Shinagawa, Acta Mater. **66**, 360 (2014)
[3] S. Mazur, D. Plazek, Prog. Org. Coat. **24**, 225 (1994)
[4] R. Fuchs, T. Weinhart, M. Ye, S. Luding, H.J. Butt, M. Kappl, Powders & Grains **140**, 13012 (2017)
[5] S. Berretta, Y. Wang, R. Davies, O.R. Ghita, J. Mater. Sci. **51**, 4778 (2016)
[6] M. Zhao, D. Drummer, K. Wudy, M. Drexler, IT. (iJES) **3**, 28 (2015)
[7] Y.Y. Lin, C.Y. Hui, A. Jagota, J. Colloid. Interf. Sci. **237**, 267 (2001)
[8] K. Johnson, K. Kendall, A. Roberts, P. R. Soc. London. **324**, 301 (1971)
[9] S. Luding, Granul. Matter. **10**, 235 (2008)
[10] T. Weinhart, L. Orefice, M. Post, M.P. Schrojenstein, I.F.C. Denissen, D.R. Tunuguntla, J.M.F. Tsang, H. Cheng, M.Y. Shaheen, H. Shi, P. Rapino, E. Grannonio, N. Losacco, J. Barbosa, L. Jing, J.E. Alvarez, S. Roy, W.K. den Otter, A.R. Thornton, Comput. Phys. Commun. **249**, 107129 (2020)
[11] P. Hejmady, L.C. Van Breemen, P.D. Anderson, R. Cardinaels, Soft Matter. **6**, 1373 (2019)
[12] H. Cheng, T. Shuku, K. Thoeni, P. Tempone, S. Luding, V. Magnanimo, Comput. Method. Appl. M. **350**, 268 (2019)